RSC Advances

PAPER

View Article Online
View Journal | View Issue

Cite this: *RSC Adv.*, 2019, **9**, 27702

Super-robust superamphiphobic surface with anti-icing property†

Huanhuan Wang, Haitao Lu and Xia Zhang *

Received 2nd July 2019
Accepted 20th August 2019

DOI: 10.1039/c9ra04997e

rsc.li/rsc-advances

Compared with superhydrophobic surfaces, superamphiphobic surfaces have a wider commercially availability. However, the initially fragile nature of micro or nano-structures hinders the large-scale applications of superamphiphobic surfaces. In this work, we report free-standing monoliths with durable superamphiphobic properties not only in the outer layer surfaces but also extending throughout the whole volume, which will demonstrate permanent superamphiphobicity. The monolith surface can repel a series of organic solutions with a surface tension as low as 36.4 mN m^{-1}, and display good self-cleaning effect toward to blood or viscous mud. In addition, the monolith can maintain the superhydrophobicity no matter whether facing corrosive solution attack or mechanical abrasion, indicating the excellent chemical and mechanical properties. The monolith surfaces also display delayed-icing property and easy de-icing process.

1. Introduction

Superamphiphobicity is an effect where surface roughness and surface chemistry combine to generate surfaces which are both superhydrophobic and superoleophobic, *i.e.*, contact angles greater than 150° along with low contact angle hysteresis not only towards probing water but also for low surface tension 'oils'.[1] Superamphiphobic surfaces that exhibit both water-repellent and oil-repellent properties, especially with a contact angle for both water and oil at 150° or above, have attracted much attention in practical applications of water repellency, self-cleaning,[2,3] anti-freezing,[4–6] biological and organic contamination prevention,[7,8] and fingerprint-resistant touch-screen devices.[9] The preparation of superamphophobic surfaces presents a greater challenge since lipophilic liquids such as cooking oils have a lower surface tension compared to that for water.[10–12] Meanwhile, textured surface required for superamphiphobic surface exhibits roughness on both the nanometer and the micrometer scales.[13,14] So far, many methods have been developed to meet this demand for hierarchical roughness in the quest for superamphiphobic surface.[15–17] However, the fragile nature of the textured surface is easily destroyed, which hinders their large-scale applications such as for structural materials. It is still a challenge to fabricate a robust superamphiphobic surface.[18–20]

Superhydrophobic and superoleophobic bulk materials with features in the nanoscale are proposed as a new concept in designing damage-tolerant superhydrophobic and superoleophobic materials.[21] Bulk monoliths possessing low surface-energy microstructures extending throughout its whole volume are regarded as good candidate for damage tolerant superamphiphobicity. When the uppermost layer is damaged or removed upon scrape abrasion, the newly exposed rough surface with low surface-energy is also water-repellent, thereby making the superamphiphobic property permanent.[22] In our previous work,[23] we presented a general method to fabricate super-robust superhydrophobic blocks through compressing nanoparticles and a series of polymers. These free-standing blocks are independent of substrates and show high abrasion-resistant properties. In this work, we demonstrate the simple compressing method to fabricate free-standing superamphiphobic monoliths with excellent mechanical and chemical stability. The obtained monoliths show a series of liquid repellency and self-cleaning properties. The ice accretion and deicing process on the obtained water-repellency surfaces also have been investigated, and it is found that the melt icing droplet can easily slide away from the surface. Not that a slight external force can make the ice droplet leave the monolith surface, which means that the deicing process is much easier compared with the hydrophilic surface.[24]

2. Experimental section

2.1 Fabrication of superamphiphobic free-standing monoliths

Hydrophobic SiO_2 nanoparticles were prepared according to our previous work.[25] Hydrochloric acid (25 mL, 0.18 M) was added into the Na_2SiO_3 water solution (50 mL, 0.15 M). After half of the hydrochloric acid had been added 1,1,1,3,3,3-

National & Local Joint Engineering Research Center for Applied Technology of Hybrid Nanomaterials, Henan University, Kaifeng 475004, PR China. E-mail: xia.zhang@ucl.ac.uk

† Electronic supplementary information (ESI) available. See DOI: 10.1039/c9ra04997e

hexamethyldisilazane (HMDS, 25 mL, 12.5 mM) was added dropwise to the Na_2SiO_3 water solution together with the remaining hydrochloric acid. The resulting suspension was stirred for 4 h at 60 °C, and then it was separated into two phases upon cooling to room temperature, with white foam floating at the top of the liquid phase. The foam was purified by filtration and cleaned repeatedly using a solution containing water and ethanol, then dried in vacuum at room temperature for 24 h to get the TMCS-functionalized SiO_2 powder.

The superamphiphobic monoliths were fabricated by mixing SiO_2 powder and perfluorotriamylamine (FC-70) at a 5 : 3 (w/w) ratio and heated at 60 °C for 6 h. After that, the mixture was grinded in mortar for 20 min to get a waxy mixture powder. Then the powder was pressed at 30 MPa at room temperature on a mold to get a free-standing monolith, and the monolith became to superamiphobic when the surface layer was removed.

2.2 Chemical characterization

Fourier transform infrared spectra (FTIR) were recorded with a vertex70 FT-IR spectrophotometer (Bruker Spectrum Instruments, Germany) in the wavenumber range of 400–4000 cm^{-1}. Field-emission scanning electron micro-scope (FESEM) images were obtained on JSM-6701F, both with Au-sputtered specimens. TG measurements were done with NETZSCH STA 449C using a dynamic heating rate of 10 °C min^{-1} (N_2). The contact angles (CA) and sliding angles (SA) and liquid surface tension were measured with optical contact angle measuring instrument DSA100S (Germany KRUSS) at ambient temperature, CA and SA were measured with a 4 μL distilled water droplet, surface tension is measured by pendant drop method. CA and SA were obtained by selecting five different positions on the sample surface. The optical photographs were taken with a digital camera (Nikon, P600).

2.3 Durability tests

There are four independent test methods to measure the durability of the sample, sandpaper abrasion test, ultraviolet accelerated aging, simulated outdoor rain and high temperature test. Superamphiphobic monolith was abraded by sandpaper (SiC, 220 Cw). During abrasion, the samples were loaded with a 32 g weights with the abrasive area of 7 cm^2. The original mass of the superamphiphobic monolith was 0.7 g. CA and SA of water (WCA, WSA) and ethylene glycol (EGCA, EGSA) were measured and calculated when the samples were abraded after every 120 cm of travel. Ultraviolet resistance of the samples was tested in an ultraviolet accelerated aging test box (LUV-II, Shanghai Pushen Chemical Machinery, China). The method of simulating outdoor rain is to spray water droplets on the surface of samples under ultraviolet irradiation. There is a row of nozzles that sprayed water droplets once every second below the UV lamp (20 W, 313 nm) at a distance of 1 cm. The distance between the nozzle and the sample was 8 cm, and the distance between the UV lamp and the sample was 9 cm. The simulation experiment was also carried out in an ultraviolet accelerated aging test chamber. The high temperature performance test was carried out by calcining the sample in an energy-saving box type electric furnace (Tianjin Zhonghuan Electric Furnace Corp.) at different temperatures for 1 h, and the heating rate is 10 °C min^{-1}.

2.4 Corrosion resistant characterization

Two independent methods were used to study if the samples superhydrophobicity has degradation because of the exposure to strong acid or strong alkali. In the first method, an acidic (pH = 1) or alkali (pH = 14) liquid droplet was dropped on the sample surface and the evolution of contact angle was studied as a function of time of corrosive droplet contact with the monolith. In the second method, the sample was soaked in strong acidic (pH = 1) and alkali (pH = 14) solution for a certain time, respectively. After a definite time of immersion, the sample was taken off the corrosive liquids, and a water or ethylene glycol droplet was dropped on the surface to investigate the influence of the corrosive solution on the wettability. The contact angle and sliding angle of water and glycol droplets were recorded. For adjusting pH value of the aqueous solutions, HCl and NaOH were used for acidic and alkali solutions.

2.5 Anti-icing performance tests

The sample was placed in a transparent quartz container and the temperature probe was exposed to the surface of the sample, then the entire device was subjected to cyclic condensation to cool down. Water droplets were dropped on the surface of the sample when the temperature drops to the desired temperature, then process monitoring was performed. The icing samples were taken after frozen for 1 h at the measured temperature (−6 °C, −8 °C, −10 °C), and the melting process was continued at room temperature (27 °C). The icing and melting process on the glass surface were consistent with the sample. The de-icing experiment was carried out after freezing the sample at −10 °C for 2 h.

3. Results and discussions

3.1 Liquid repellency of the monoliths

The obtained monoliths can repel a series of organic solution with different surface tension, and the relationship between the contact angle, sliding angle and the solution surface tension is shown in Fig. 1. It can be seen that contact angle increases with the solution surface tension, while the sliding angle decreases with the surface tension. The monoliths show superoleophobicity to the organic solutions with surface tension as low as 36.4 mN m^{-1}, and the liquid contact angle is about 155° and sliding angle is about 32°.

3.2 Characterization and durability of the superhydrophobic monoliths

Fig. 2(a) and (b) shows the water and ethylene glycol droplets sitting on the monolith surface with a static water contact angle (CA) of 171 ± 1° and 167 ± 1°, respectively. The monolith is so amphiphobic that the water or ethylene glycol droplets readily slide away from the surface therefore showing excellent self-

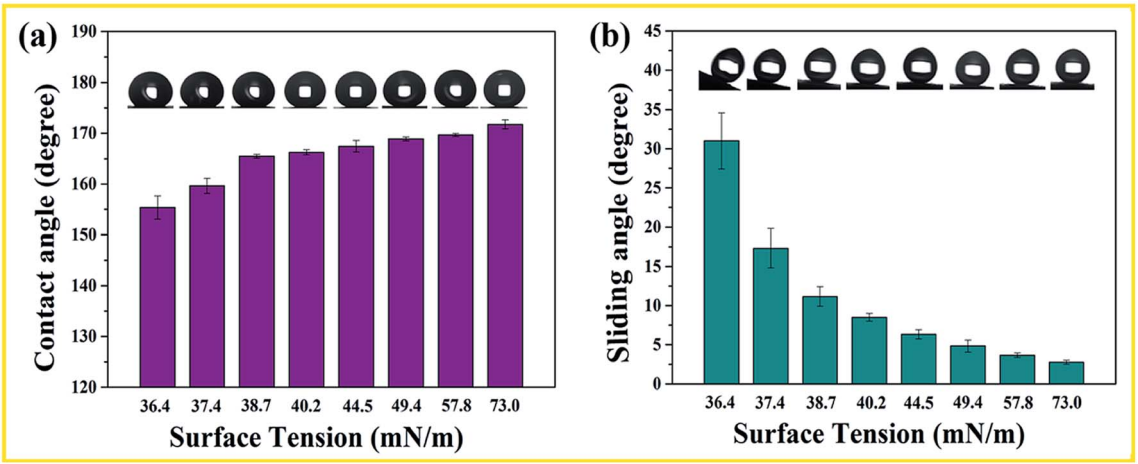

Fig. 1 Contact angle (a) and sliding angle (b) as a function of different solution surface tension.

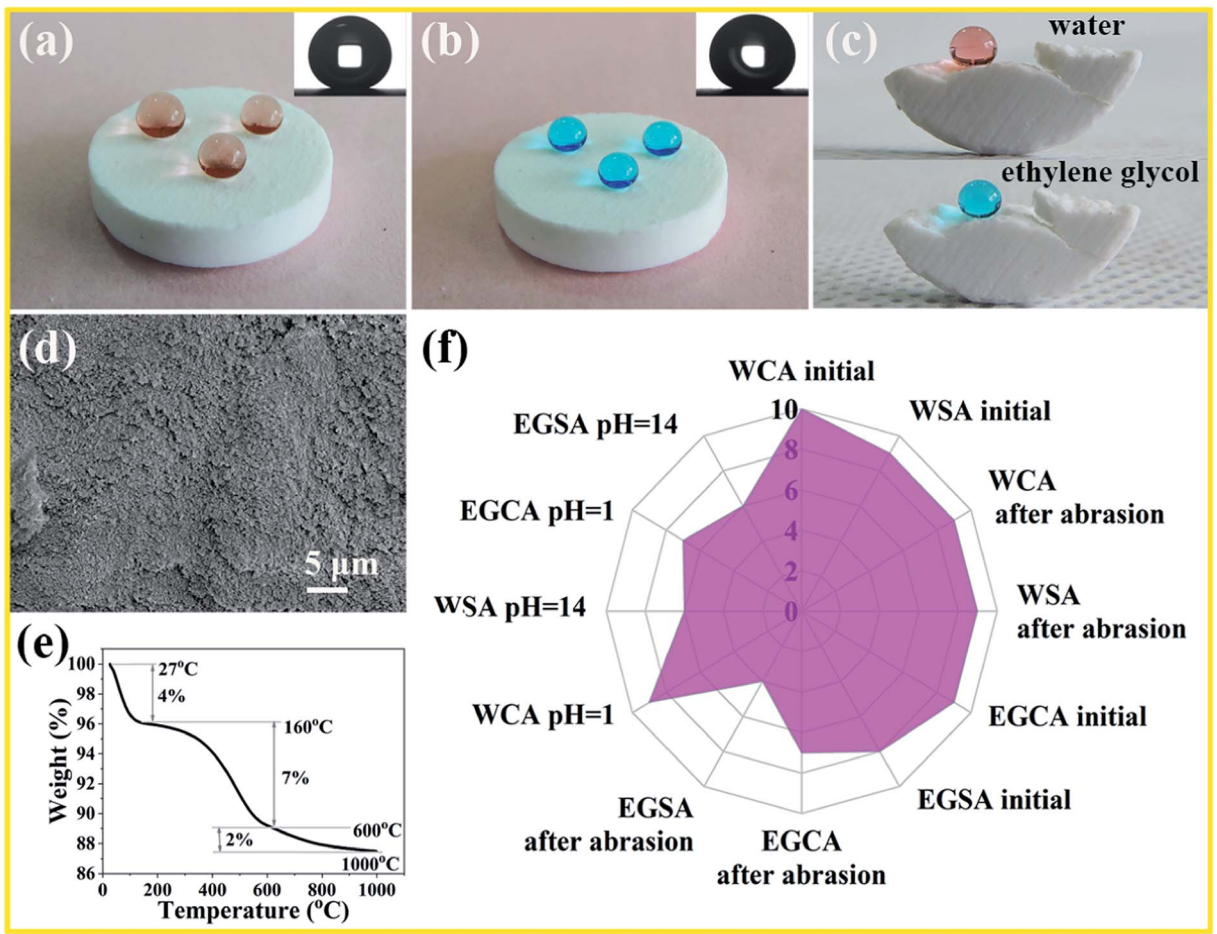

Fig. 2 Optical image of water (a) and (b) ethylene glycol droplets sitting on the obtained monolith surface with contact angle about 171 ± 1° and 167 ± 1°. (c) Water (upper) and ethylene glycol (lower) test at the cross-sectional crack to show superamphiphobicity inside the monoliths. SEM (d) and TG (e) analysis of the obtained monoliths. (f) Radar diagrams of the superamphiphobic monoliths. Herein, "WCA initial" and "WSA initial" refer to the water contact angles and water sliding angles of the samples without any mechanical and chemical tests. "WCA after abrasion" and "WSA after abrasion" refer to the water contact angles and water sliding angles that were measured after the sample being abraded for 1500 cm. "EGCA initial" and "EGSA initial" refer to the ethylene glycol contact angles and ethylene glycol sliding angles of the sample before any mechanical and chemical tests. "EGCA after abrasion" and "EGSA after abrasion" refer to the ethylene glycol contact angles and ethylene glycol sliding angles that were measured after the sample being abraded for 1500 cm (32 g loads, SiC, 220 Cw sandpaper). "WCA pH = 1 and EGCA pH = 1" refer to the water and ethylene glycol contact angles measured after 50 min acid attack. "WCA pH = 14 and EGCA pH = 14" refer to the water and ethylene glycol contact angles measured after 50 min alkali attack.

cleaning properties (Video S1 and S2†). Since the low surface energy and microstructures extending throughout the whole volume of the monoliths, the monolith internal parts also demonstrate superoleophobicity and it is clear that the ethylene glycol droplets on the interior area retain spherical shapes with oil contact angle about 166 ± 1° (Fig. 2(c)). The wettability of the monoliths under oil (liquid paraffin) was also investigated, and it is found that the water contact angle is 174 ± 1° (Fig. S1 and Video S3†), which demonstrates that the monolith is also superhydrophobic under oil. In combination with FT-IR (Fig. S2†) analysis, the hydrophobic $-CH_3$ was successfully modified on the surface of the SiO_2 nanoparticles. From SEM image (Fig. 2(d)), it is clear that the surface is rough, which is a requirement for superamphiphobicity. From element distribution maps of the superamphiphobic monolith (Fig. S3†), it can be clearly seen that SiO_2 and FC-70 are well-distributed in the monoliths. Thermogravimetric (TG) analysis shows that the superamphiphobic monolith loss 4% of its weight before 200 °C, indicating the thermal stability under 200 °C (Fig. 2(e)); this would meet most of the required in our daily life.

Radar diagram was used to evaluate the mechanical and chemical durability of the monoliths, and the experimental data as shown in Fig. 1(f). In the radar diagrams, we included contact angle and sliding angle of water and ethylene glycol droplet before and after sandpaper abrasion (32 g loads, SiC, 220 Cw sandpaper) about 1500 cm; water and ethylene glycol contact angle was also measured after the "strong corrosive soak test"

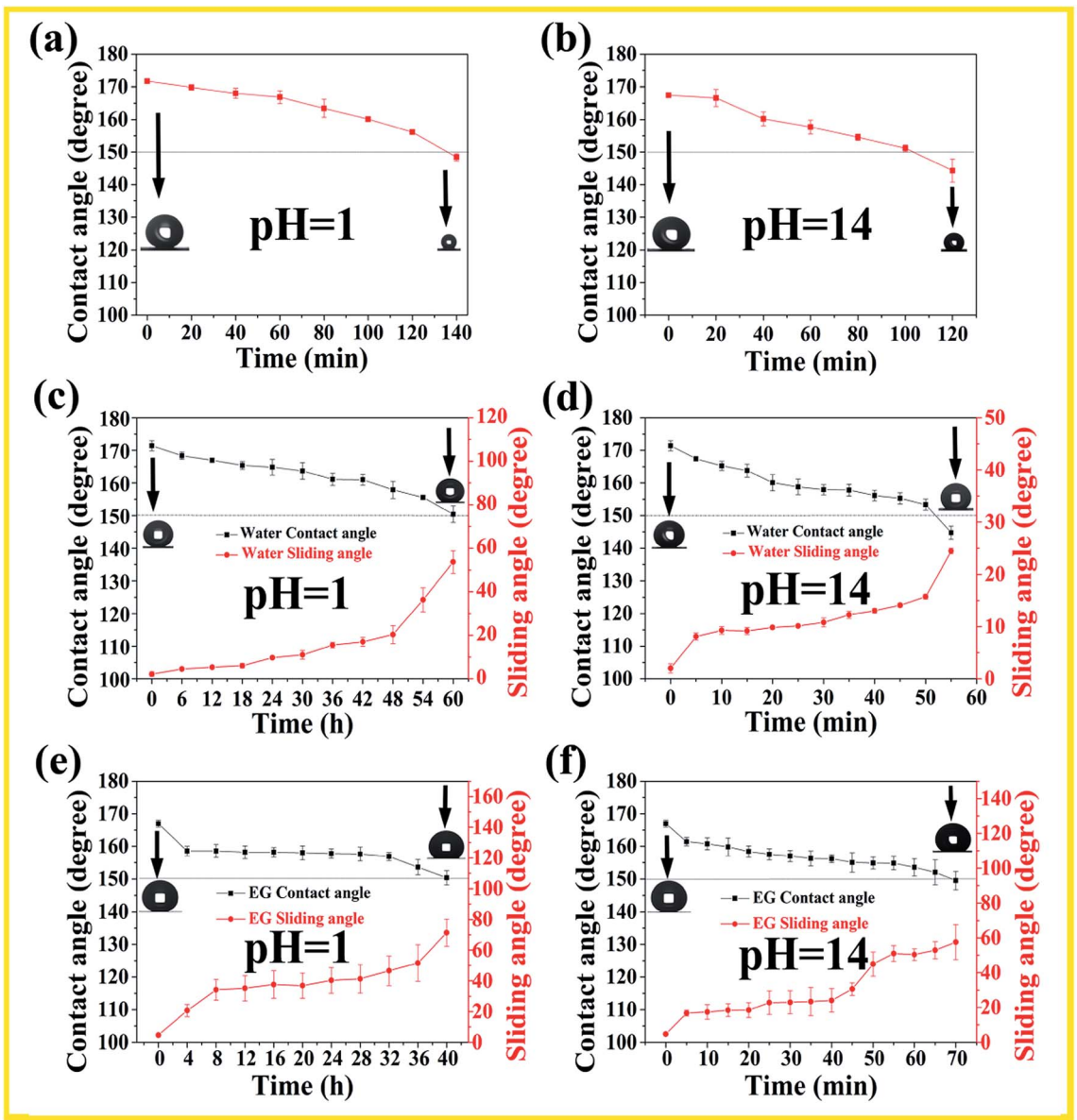

Fig. 3 (a and b) Water contact angle as a function of time in acidic/alkali droplet contact tests. (c and d) Water contact angle as a function of time in acidic/alkali soak tests. (e and f) Ethylene glycol contact angle as a function of time in acidic/alkali soak tests.

for 50 min; Table S1 in ESI† shows the rating system of the radar diagram according to the performance of the samples, and their data sheets were as shown in Table S2 (ESI†). The larger overall points that a sample achieved, the larger area on the radar diagram will be obtained, which indicates better performance. To further quantify the abrasion-resistance of the superamphiphobicity, we investigated the functional of water and EG contact angle as the abrasive distance and the detailed information was shown in Fig. S5(a and b).† For water droplet, the abrasion shows no obvious influence on the contact angle and sliding angle; the contact angle maintains about 170° and the sliding angle less than 4° as the abrasive distance goes. As far as the lower surface tension liquid, such as ethylene glycol, the contact angle decreases and the sliding angle increases as the abrasive distance goes. However, the monolith keeps the superamphiphobic properties after 1500 cm abrasive distance, demonstrating the excellent abrasion resistance.

Chemical stability is very important for superamphiphobic surface facing the real world application. Two independent methods were employed to further investigate the anti-corrosion properties of the surface, and the detailed information was shown in Fig. 3. In the "droplet test", strong acid and alkali droplets were dropped on superamphiphobic monolith surface, respectively, as shown in Fig. 3(a) and (b). It is noted that the water droplets became smaller due to the evaporation, and as acid/alkali contact time increased, the CAs of acid/alkali droplets slightly decreased. Despite slight decreases in the contact angle with contact, the monolith can maintain its

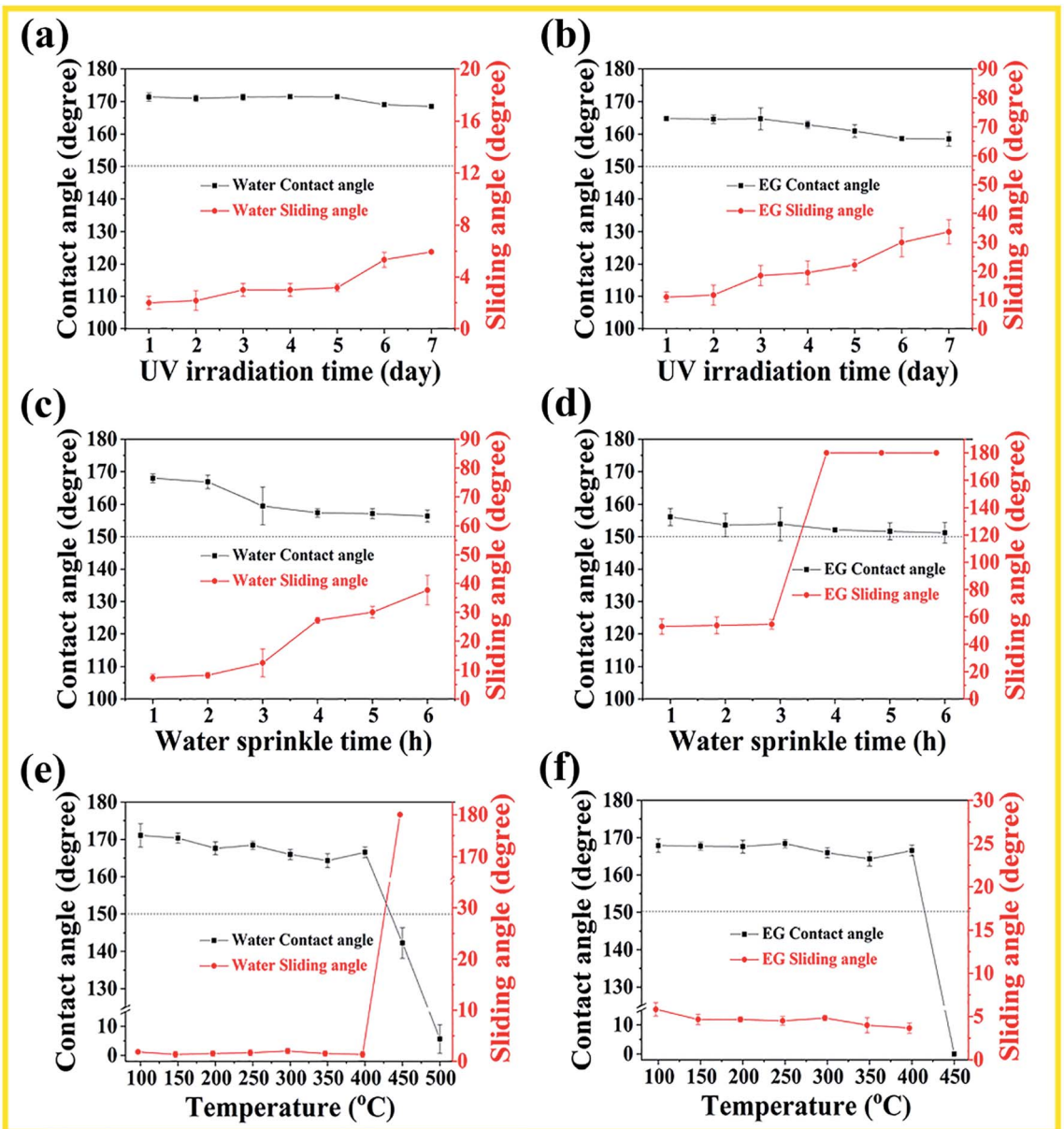

Fig. 4 Stability tests. (a and b) Contact angle and sliding angle in UV accelerated aging tests at 40 °C; (c and d) contact angle and sliding angle as a function of time in water washout tests. (e and f) Water/EG contact angle and sliding angle on superamphiphobic monoliths surface after being calcined at different temperature.

superhydrophobicity under 100 min corrosive attack. In a more aggressive test, the monoliths were immersed into acid (pH = 1) and alkali (pH = 14) baths, as shown in Fig. 3(c–f). Although the water/ethylene glycol contact angle decreases and sliding angle increases with the increasing soak time, the monoliths can retain the superamphiphobicity in a strong corrosive solution for more than 40 min, and this is very important for superamphiphobic monoliths in our daily life use.

In consideration of outdoor applications, the monoliths surface is expected to be UV resistant. The obtained monoliths were placed in an UV accelerated weathering tester (wavelength: 313 nm) for 7 days to evaluate their UV resistance. The samples were taken out at a specific time each day for the WCA and WSA measurements. As shown in Fig. 4(a) and (b), under UV irradiation for 7 days, the water CA value and ethylene glycol CA value are larger than 150°. The water SA value maintains below than 10° during the process, indicating excellent resistance to UV light. However, the ethylene glycol SA value increases to about 32° after being exposed under UV irradiation for 7 days, which indicates the UV irradiation has a deep effect on the oil adhesion property.

Superamphiphobic surfaces are usually subject to rainwater impact because the poor surface mechanical stability. In consideration of outdoor applications, we investigated the superamphiphobic durability of the monoliths surface facing the rainwater impact. As shown in Fig. 4(c) and (d), after exposure at rain washout for 6 h, the monolith surface still maintain superhydrophobic and superoleophobic properties, and the SA value for water and ethylene glycol increases with washout time. It is notice that ethylene glycol sliding angle increases to 180°, indicating the high adhesion of the monolith surface. In order to restore the original superhydrophobicity, the water impact layer just needs to be removed by mechanical abrasion to expose the interior of the superamphiphobic monolith material. To further indicate the thermal stability, the monolith was calcined at different temperatures for 1 h under an air atmosphere. As shown in Fig. 4(e) and (f), the superamphiphobicity has hardly changed before 400 °C, and the monolith surface retained the water and ethylene glycol CA value of >150°; water and ethylene glycol SA value of <10° during the process. It's worth noticing that when the temperature continues to rise to 500 °C, the surface wettability turns from superhydrophobic to superhydrophilic, which due to the volatilization of hydrophobic FC-70 and the breakage of long-chain alkane bonds modified on the surface of silica at a high temperature.

3.3 Self-cleaning and anti-icing properties

The superhydrophobic surfaces, like a lotus leaf, have excellent self-cleaning properties. Herein, the obtained superamphiphobic monoliths also show dirty resistance, as shown in Fig. 5 and Video S4–S6,† after vigorous stirring blood and mud for several times, the monolith remained dry and clean. Water or ethylene glycol droplets could easily take away the soil and leave the monolith surface clean (Fig. 5(k–o)).

Numerous studies have shown that surface wettability affects the nucleation time of undercooled water,[26] Hydrophilic surface is easy to be wetted with water droplets and the large contact areas will increase the possibility of nucleation, which is crucial to the icing rate. Whereas superhydrophobic surface with Cassie–Baxter state always exhibits the longest freezing delay time, due to the multitudinous air pockets between the liquid/ice and solid. The pockets sharply reduced the actual contact area and the adhesion on the surface accordingly and effectively restrained thermal conduction at low temperature. As shown in the Fig. 6(a–c) and Video S7,† after the low temperature icing-thawing process, the superhydrophobic monolith surface

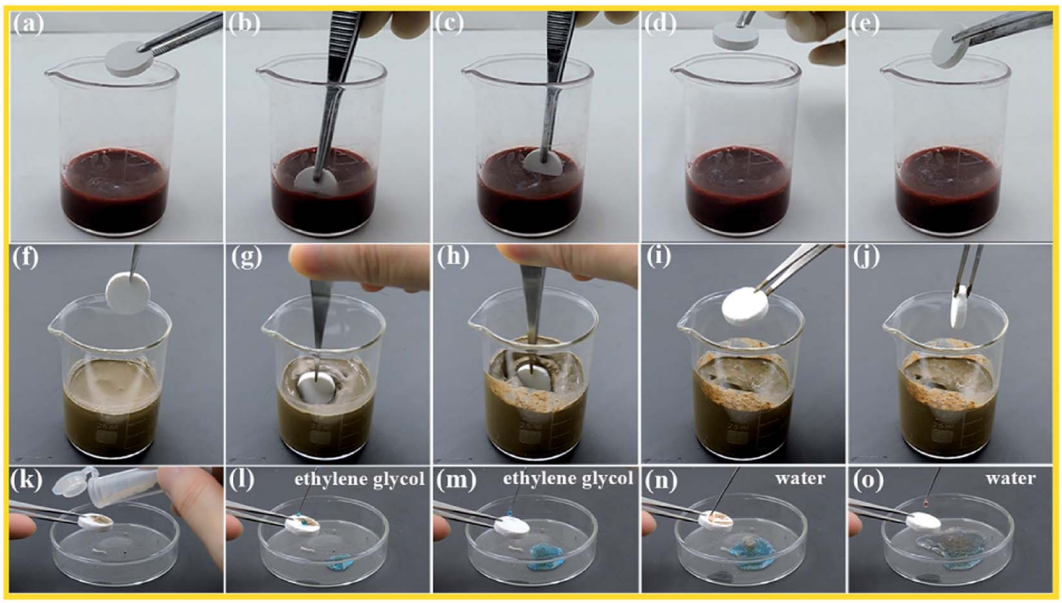

Fig. 5 Self-cleaning properties of the obtained monoliths. No adhesion after dipping and stirring in blood (a–e) and mud (f–j) for several times. (k–o) water or ethylene glycol droplet can bounce and take away the dirt.

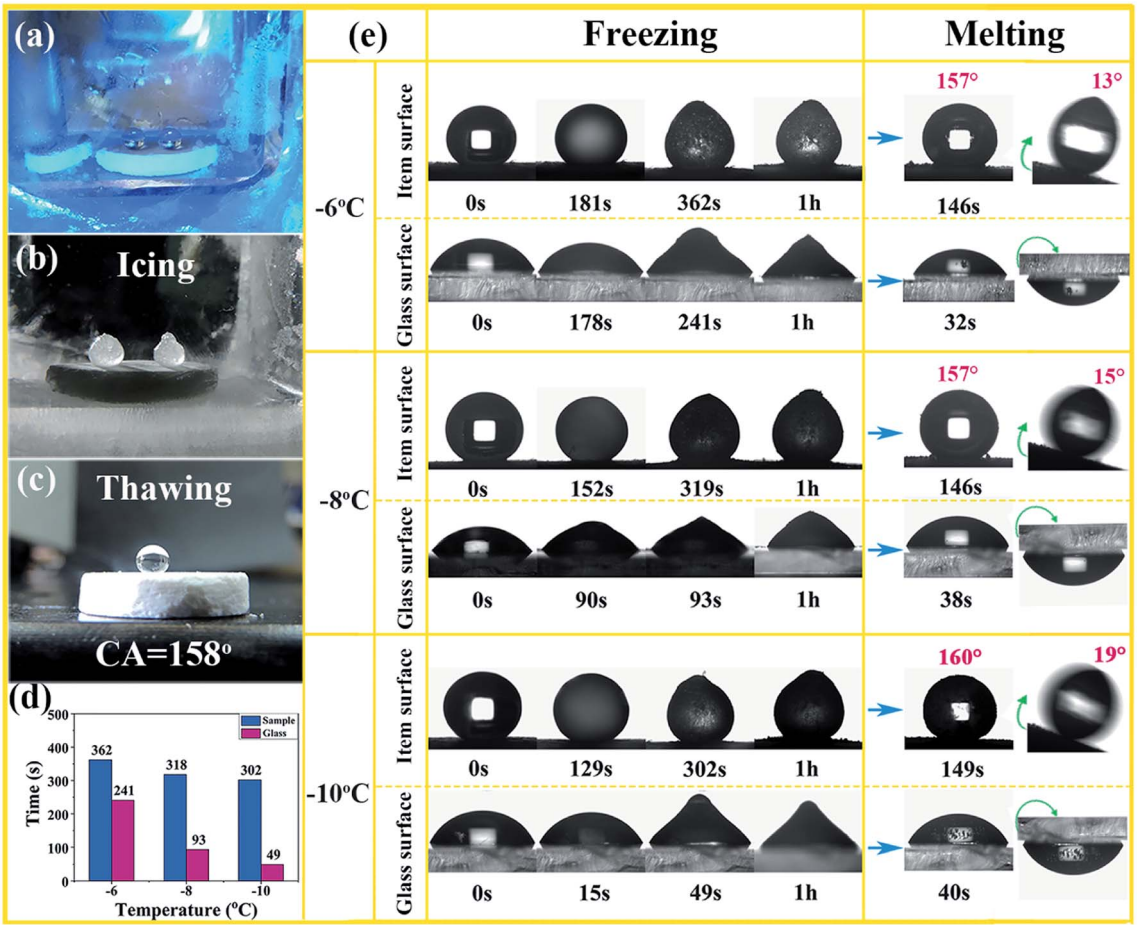

Fig. 6 Anti-icing process at different low temperatures (a) at initial time; (b) freezing; (c) after being melted at room temperature. (d) The total icing time for a droplet at different low temperatures. (e) Detailed ice formation and thawing process on superhydrophobic monolith and hydrophilic glass surface.

remains contact angle about 158°. From Fig. 6(d), it is clear that the superhydrophobic monolith surface can delay the icing time compared with the hydrophilic glass surface. For example, water droplet icing time is only 49 s on hydrophilic glass surface at −10 °C. However, on superhydrophobic monolith surface, it needs 302 s. Note that the icing can be get rid of from the monolith surface under a slight external force which means the easier deicing process. As shown in Video S8,† it is clear that the water droplets froze on a large area and adhered firmly to the hydrophilic glass surface after freezing at −10 °C for 1 h, and it is not easy to get rid of the ice beads. Conversely, spherical ice beads can be removed easily from superhydrophobic monolith surface under a slight external tap. Fig. 6(e) shows the detailed processes of icing and thawing on superhydrophobic monoliths and hydrophilic glass surfaces. After having been frozen for 1 h, the sample was put into ambient environment to melt at room temperature. The melting process need longer time on superamphiphobic monolith surfaces than on the hydrophilic glass surfaces, which indicates that the air pockets are a disadvantage of melting. However, the melted droplet has a high contact angle value (more than 150°) on the monolith surface and a lower sliding angle (lower than 20°), and the melted droplet can slide away easily from the monolith surface and no wet was left. Whilst, the melted water droplet adheres on glass surface even being turned upside down, which also means it is not easy of the de-icing process on hydrophilic glass surface.

4. Conclusions

In conclusion, a simple and easy method was developed to make free-standing monoliths with super-robust superamphiphobic properties. The monoliths surface can repel the different organic solution with the surface tension as low as 36.5 mN m^{-1} and resists adhesion by blood and mud. The monolith shows a remarkable robustness and can maintain the superhydrophobic and superoleophobic properties to harsh environments such as strong corrosion, UV irradiation, high temperature, and long-term water droplet impact. In addition, the superamphiphobic monolith surface demonstrates the performance of delayed icing, and the frozen ice droplets can be removed under a minimal force, showing the characteristics of easy de-icing. This method provides a new thinking for the fabrication of super-robust superamphiphobic surface and

yield a prospective candidate for various practical applications in real world.

Conflicts of interest

There are no conflicts to declare.

Acknowledgements

This project is supported by National Natural Science Foundation of China (Grant No. 51875173) and the innovative talents promotion plan of Henan province (20HASTIT003).

References

1 Z. L. Chu and S. Seeger, Superamphiphobic surfaces, *Chem. Soc. Rev.*, 2014, **43**, 2784–2798, DOI: 10.1039/c3cs60415b.

2 X. Deng, L. Mammen, H. J. Butt and D. Vollmer, Candle soot as a template for a transparent robust superamphiphobic coating, *Science*, 2012, **335**, 67–70, DOI: 10.1126/science.1207115.

3 V. A. Ganesh, S. S. Dinachali, H. K. Raut, T. M. Walsh, A. S. Nair and S. Ramakrishna, *RSC Adv.*, 2013, **3**, 3819–3824, DOI: 10.1039/c3ra22968h.

4 P. Tourkine, M. L. Merrer and D. Quéré, Delayed Freezing on Water Repellent Materials, *Langmuir*, 2009, **25**, 7214–7216, DOI: 10.1021/la900929u.

5 M. He, Q. L. Zhang, X. L. Zeng, D. P. Cui, J. Chen, H. L. Li, J. J. Wang and Y. L. Song, Hierarchical Porous Surface for Effi ciently Controlling Microdroplets' Self-Removal, *Adv. Mater.*, 2013, **25**, 2291–2295, DOI: 10.1002/adma.201204660.

6 S. A. Kulinich and M. Farzaneh, Ice adhesion on superhydrophobic surfaces, *Appl. Surf. Sci.*, 2009, **255**, 8153–8157, DOI: 10.1016/j.apsusc.2009.05.033.

7 C. F. Jin, Y. F. Jiang, T. Niu and J. G. Huang, Cellulose-based material with amphiphobicity to inhibit bacterial adhesion by surface modification, *J. Mater. Chem.*, 2012, **22**, 12562–12567, DOI: 10.1039/c2jm31750h.

8 M. Guo, B. Ding, X. H. Li, X. L. Wang, J. Y. Yu and M. R. Wang, *J. Phys. Chem. C*, 2010, **114**, 916–921, DOI: 10.1021/jp909672r.

9 H. Kondo, L. Sungkil and H. Hanaoka, Durable Anti-Smudge Materials for Display Terminals, *Tribol. Trans.*, 2008, **52**, 29–35, DOI: 10.1080/10402000802044357.

10 G. W. Zhang, J. W. Hu, G. J. Liu, H. L. Zou, Y. Y. Tu, F. Li, S. Y. Hu and H. S. Luo, Bi-functional random copolymers for one-pot fabrication of superamphiphobic particulate coatings, *J. Mater. Chem. A*, 2013, **1**, 6226–6237, DOI: 10.1039/c3ta10722a.

11 K. Tsujii, T. Yamamoto, T. Onda and S. Shibuichi, Super Oil-Repellent Surfaces, *Angew. Chem., Int. Ed.*, 1997, **36**, 1011–1012, DOI: 10.1002/anie.199710111.

12 K. Rykaczewski, A. T. Paxson, M. Staymates, M. L. Walker, X. D. Sun, S. Anand, S. Srinivasan, G. H. McKinley, J. Chinn, J. H. J. Scott and K. K. Varanasi, Dropwise Condensation of Low Surface Tension Fluids on Omniphobic Surfaces, *Sci. Rep.*, 2014, **4**, 4158, DOI: 10.1038/srep04158.

13 T. Fujii, H. Sato, E. Tsuji, Y. Aoki and H. Habazaki, Important role of nanopore morphology in superoleophobic hierarchical surfaces, *J. Phys. Chem. C*, 2012, **116**, 23308–23314, DOI: 10.1021/jp305078t.

14 L. L. Cao, T. P. Price, M. Weiss and D. Gao, Super water- and oil-repellent surfaces on intrinsically hydrophilic and oleophilic porous silicon films, *Langmuir*, 2008, **24**, 1640–1643, DOI: 10.1021/la703401f.

15 Z. G. Tang, D. W. Hess and V. Breedveld, Fabrication of oleophobic paper with tunable hydrophilicity by treatment with non-fluorinated chemicals, *J. Mater. Chem. A*, 2015, **3**, 14651–14660, DOI: 10.1039/C5TA03520A.

16 Z. Geng and J. J. He, An effective method to significantly enhance the robustness and adhesion-to-substrate of high transmittance superamphiphobic silica thin films, *J. Mater. Chem. A*, 2014, **2**, 16601–16607, DOI: 10.1039/c4ta03533j.

17 J. L. Yong, F. Chen, Q. Yang, J. L. Huo and X. Hou, Superoleophobic surfaces, *Chem. Soc. Rev.*, 2017, **46**, 4168–4217, DOI: 10.1039/c6cs00751a.

18 T. Verho, C. Bower, P. Andrew, S. Franssila, O. Ikkala, R. H. A. Ras, S. Franssila, O. Ikkala and R. H. A. Ras, Mechanically Durable Superhydrophobic Surfaces, *Adv. Mater.*, 2011, **23**, 673–678, DOI: 10.1002/adma.201003129.

19 X. T. Zhu, Z. Z. Zhang, X. H. Men, J. Yang, K. Wang, X. H. Xu, X. Y. Zhou and Q. J. Xue, Robust superhydrophobic surfaces with mechanical durability and easy repairability, *J. Mater. Chem.*, 2011, **21**, 15793–15797, DOI: 10.1039/c1jm12513c.

20 G. W. Zhang, S. D. Lin, I. Wyman, H. L. Zou, J. W. Hu, G. J. Liu, J. D. Wang, F. Li, F. Liu and M. L. Hu, Robust superamphiphobic coatings based on silica particles bearing bifunctional random copolymers, *ACS Appl. Mater. Interfaces*, 2013, **5**, 13466–13477, DOI: 10.1021/am404317c.

21 H. Jin, X. L. Tian, O. Ikkala and R. H. A. Ras, Preservation of superhydrophobic and superoleophobic properties upon wear damage, *ACS Appl. Mater. Interfaces*, 2013, **5**, 485–488, DOI: 10.1021/am302541f.

22 X. Zhang, W. Z. Zhu, G. J. He, P. Y. Zhang, Z. J. Zhang and I. P. Parkin, Flexible and mechanically robust superhydrophobic silicone surfaces with stable Cassie-Baxter state, *J. Mater. Chem. A*, 2016, **4**, 14180–14186, DOI: 10.1039/c6ta06493k.

23 X. Zhang, D. F. Zhi, L. Sun, Y. B. Zhao, M. K. Tiwari, C. J. Carmalt, I. P. Parkin and Y. Lu, Super-durable, non-fluorinated superhydrophobic free-standing monoliths, *J. Mater. Chem. A*, 2018, **6**, 357–362, DOI: 10.1039/c7ta08895g.

24 M. J. Kreder, J. Alvarenga, P. Kim and J. Aizenberg, Design of anti-icing surfaces: smooth, textured or slippery?, *Nat. Rev. Mater.*, 2016, **1**, 15003, DOI: 10.1038/natrevmats.2015.3.

25 D. F. Zhi, Y. Lu, S. Sathasivam, I. P. Parkin and X. Zhang, Large-scale fabrication of translucent and repairable superhydrophobic spray coatings with remarkable mechanical, chemical durability and UV resistance, *J. Mater. Chem. A*, 2017, **5**, 10622–10631, DOI: 10.1039/c7ta02488f.

26 Z. G. Guo and Q. Li, Fundamentals of icing and common strategies for designing biomimetic anti-icing surfaces, *J. Mater. Chem. A*, 2018, **6**, 13549–13581, DOI: 10.1039/c8ta03259a.